

Nanoscale

Accepted Manuscript



This is an *Accepted Manuscript*, which has been through the Royal Society of Chemistry peer review process and has been accepted for publication.

Accepted Manuscripts are published online shortly after acceptance, before technical editing, formatting and proof reading. Using this free service, authors can make their results available to the community, in citable form, before we publish the edited article. We will replace this *Accepted Manuscript* with the edited and formatted *Advance Article* as soon as it is available.

You can find more information about *Accepted Manuscripts* in the [Information for Authors](#).

Please note that technical editing may introduce minor changes to the text and/or graphics, which may alter content. The journal's standard [Terms & Conditions](#) and the [Ethical guidelines](#) still apply. In no event shall the Royal Society of Chemistry be held responsible for any errors or omissions in this *Accepted Manuscript* or any consequences arising from the use of any information it contains.

Metastability of the atomic structures of size-selected gold nanoparticles

Dawn M. Wells[†], Giulia Rossi[‡], Riccardo Ferrando[‡] and Richard E. Palmer^{†*}

[†]Nanoscale Physics Research Laboratory, School of Physics and Astronomy, University of Birmingham, Birmingham B15 2TT, UK

[‡]INFN and IMEM/CNR, Dipartimento di Fisica dell'Università di Genova, via Dodecaneso 33, 16146 Genova, Italy

All nanostructures are metastable – but some are more metastable than others. Here we employ aberration-corrected electron microscopy and atomistic computer simulations to demonstrate the hierarchy of metastability in deposited, size-selected gold nanoparticles (clusters), an archetypal class of nanomaterials well known for the catalytic activity which only appears on the nanometer-scale. We show that the atomic structures presented by “magic number” Au₅₆₁, Au₇₄₂ and Au₉₂₃ clusters are “locked”. They are in fact determined by the solidification which occurs from the liquid state early in their growth (by assembly from atoms in the gas phase) followed by template growth. It is quite likely that transitions from a locked, metastable configuration to a more stable (but still metastable) structure, as observed here under the electron beam, will occur during catalytic reactions, for example.

From the sintering of catalyst particles under prolonged reaction conditions¹ to the breakdown of semiconductor devices through electro-migration² and the aggregation of protein molecules in the brain³, an understanding (and control) of the hierarchical nature of metastability in nanostructured systems is central to the development of materials (and bio) technology. Gold nanoclusters have a variety of applications (current and potential) in areas such as catalysis⁴, bio-sensing⁵ and drug-delivery⁶. Both the size^{4,7} and structure^{7,8,9,10} of these particles influence their properties; therefore it is important to understand the equilibrium structures for size-specific nanoclusters, recognizing that the equilibrium in question is inherently local in nature (small particles always want to aggregate to reduce surface energy), i.e., they are metastable. It is believed that gold nanoclusters have three principle structures: the Icosahedron (Ih), the Decahedron (Dh) and face-centred cubic (fcc) (i.e. bulk-like) structures. Much theoretical^{11,12,13}, and some experimental^{14,15,16,17,18}, work has been undertaken on this problem; the general trend ascribed to many metal nanoparticles is from Ih to Dh to fcc with increasing size, though theoretical predictions for Au nanoparticles vary dramatically^{11,12,13}. Magic number clusters¹⁹, e.g. Au₅₆₁ and Au₉₂₃, present a valuable set of reference points. We show the observed isomeric abundances (even when generated under slow growth conditions) are unreliable guides to the “equilibrium” structure at a particular size. Indeed the most abundant, decahedral structures observed can be converted (by irradiation) into face-centred cubic atomic arrangements.

Here we explore and manipulate the atomic structures of size-selected gold nanoclusters with 561 ± 13 and 742 ± 17 atoms in comparison with 923 ± 23 atoms¹⁸, thereby revealing the hierarchy of atomic structures in this model system. Nanoclusters were produced under slow growth conditions, imaged using scanning

transmission electron microscopy (STEM) in high angle annular dark field (HAADF) mode (i.e., incoherent scattering^{14,20}) to achieve quasi-3D atomic resolution, and identified by comparison with multiple electron scattering simulations for icosahedral (Ih), face-centred cubic (fcc) and decahedral (Dh) geometries. A key finding is that the proportion of the different isomers is, to within experimental accuracy, *exactly the same* for all three cluster sizes. This suggests that the cluster structures are already locked by size $N=561$ as they grow from atoms in the gas condensation process, i.e. that the structure we see at size 561 is the result of template growth on smaller seeds. Atomistic simulations of the cluster growth by molecular dynamics confirm a competition between the Dh and fcc geometries, give similar isomer ratios to those observed and, crucially, demonstrate the absence of solid-solid transitions during the growth process. Video imaging of Au_{561} clusters during STEM irradiation shows a systematic tendency for decahedral clusters (originating from smaller seeds) to convert into fcc structures, which appear to be the most stable isomers (if one can create them).

Figure 1 shows examples of structures identified by comparison between the electron microscope experiments and the electron scattering simulations; the HAADF STEM image is shown on the left and the corresponding simulated image on the right. The clusters are classified into 4 categories: Ih, fcc, Dh and unidentified or amorphous (UI/A). All possible truncations of fcc and Dh clusters are included within these categories. Figures 1a)-c) show Au_{561} clusters with Ih, fcc and Dh structures, respectively, and corresponding simulations in f)-h); all these clusters were found to be orientated on or near a high symmetry axis. Figure 1d) shows a Dh Au_{561} cluster which is not orientated along a high symmetry axis, and the corresponding simulation for this angle of orientation in i).

The structures of clusters were identified visually with reference to a simulation 'atlas'. The simulation 'atlas' contains multislice, electron scattering, simulated images²¹ for a complete range of cluster orientations. The simulations were performed on geometrical models of the icosahedron, Ino-decahedron and cuboctahedron. It was not possible to identify all clusters, this was due to a variety of reasons, such as: instability under the electron beam, image quality, and in some cases (particularly for Au_{309}) there was no structure; figure 1e) shows an example of a Au_{561} cluster which is amorphous (in the sense that it does not match any orientation of the simulated structures).

Figure 2 presents the percentages of nanoclusters lying within the four categories (Ih, fcc, Dh and UI/A) for Au_{561} and Au_{742} with the data for Au_{923} from Ref. 18 (averaging over the two sets included therein). In all cases the clusters were produced with magnetron power 10W and condensation length 250mm (slow growth conditions). For Au_{561} (Au_{742}) 189 (147) clusters were imaged. The Dh structure is most commonly observed (43%), followed by fcc (36%), with only 2% of structures identified as Ih. For Au_{923} the most common structure is again Dh (42%), followed by fcc (31%), and Ih (4%); within the estimated experimental errors these proportions are statistically identical. The same is true for the Au_{742} clusters (chosen to lie midway between the two magic numbers), where the proportions are 46% Dh, 37% fcc, and 3% Ih. For Au_{561} , Au_{742} and Au_{923} the abundance ratios fcc:Dh are 0.83 ± 0.16 , 0.79 ± 0.18 and 0.74 respectively. The errors quoted are statistical counting errors.

Why do the same proportions of the two main isomers appear at the three quite different gold cluster sizes investigated? It might reasonably be argued that the fcc and Dh structures compete with each other over the size range reported here, such that the relative stability oscillates with size and either motif may present the lowest free energy for any particular size¹². On that basis one might encounter the occasional coincidence in the isomer proportions in selecting two sizes at random. However to get the same proportions for three sizes seems more than a coincidence (and this is proved by the atomic manipulation experiments reported below). The alternative explanation is that the structures of individual clusters within the population are already ‘locked’ (or ‘frozen in’) by size by 561, such that subsequent growth by addition of atoms is templated onto smaller seed structures, preserving the structural motif. Beyond a certain size, the activation energy required to rearrange many or all of the atoms in the cluster to achieve a final, lower energy configuration may be prohibitive at the growth temperatures employed.

Many theoretical studies predicted that the icosahedron (Ih) should be the most stable state for small clusters in the sub 10nm size range^{11, 12, 13}. This is because the high surface to volume ratio at small sizes makes it favourable to minimise the surface energy over the internal strain. The Ih has large internal strain (compared with Dh and fcc) due to the displacement of the atoms from their bulk crystal locations, but a lower surface energy due to the almost spherical shape and (111) close-packed facets^{12, 13}. The results we show contradict these predictions. On the contrary, it is also reported¹² that, even at very small (~ 400 atoms) sizes, the icosahedron is not the equilibrium structure for gold clusters, rather the fcc structure is most favourable. This is attributed to the large energy associated with displacing atoms from the bulk crystalline structure of gold¹².

In order to investigate in more depth, and in a quantitative fashion, the possible growth mechanisms of the clusters, including the concept of template growth, we studied the growth of gold nanoparticles (by condensation in the vapour phase) via molecular dynamics simulations. The atomistic interaction potential used in the simulation is a semi-empirical, tight-binding based potential^{22,23}. For each growth temperature (400K, 500K, and 600K) we ran 12 independent simulations, starting from size 13 up to size 923. Snapshots from typical growth sequences are shown in Fig. 3. All simulations show some common features. Gold clusters are liquid for small sizes, and solidify while growing, because the melting point depression is size-dependent. For T=400 and 500 K solidification is below size 300, whereas at 600 K solidification takes place between sizes 350 and 500. Essentially, no structural transformations during growth have been observed after solidification, with only one exception in 36 simulations. This exception is for a structure grown at 400 K, which starts as an icosahedron, transforms into an fcc structure around size 180, and then continues to grow as an fcc nanoparticle up to 1000 atoms. Therefore, the simulation results corroborate the interpretation of the experiments in terms of frozen growth in the gas phase. The growing nanoparticles solidify in a given motif and then grow by retaining the same structure up to the final size. From this point of view, gold behaves differently from silver; simulations of silver growth under the same conditions showed the occurrence of several structural transformations in the solid state²⁴.

Table 1 shows the statistical outcomes of all 36 growth simulations. The most common structure produced in the simulations is the decahedron, but the number of

fcc structures is not far behind. Very few icosahedra are produced, together with a few complicated twins that are indicated as unclassified structures. The potential energy of all fcc and Dh structures differ by less than 1 eV, while the icosahedral structures are higher in energy by a few eV. The predominance of fcc and decahedra isomers reflects the energetics that we obtain by global optimization of Au₉₂₃ clusters and that reported in Ref.12. We note the remarkable agreement between the abundances of the different structures in the experiment (see Fig. 2) and in the simulations (Table 1).

To explore directly whether the distributions of isomers we observe in the experiments are indeed metastable, as the similarity of the distributions at different sizes and the growth simulations imply, we performed continuous irradiation and imaging experiments on eighteen individual Au₅₆₁ clusters. They were irradiated by the STEM electron beam for a prolonged period of time (specifically, for a minimum of 50 frames with an acquisition time of 2.9 seconds per frame and a dose of 2.1×10^4 e⁻/Å²/frame), while any resulting structural transformations were observed (video imaging). This method was previously used to show that the icosahedral isomers of the Au₉₂₃ clusters generated under fast growth conditions were metastable¹⁵. Table 2 lists the observed initial and final structures of the clusters, and the frequency of each transition. The result is that for clusters that were initially decahedral in structure, 8/9 transformed to fcc within 50 frames, whereas for clusters that were initially fcc, 8/9 remained fcc over 50 frames. The other fcc cluster was observed to transform to Dh structure, but then transformed back to fcc. An example of a transformation ‘video’ can be found as Supplementary video S2 online. These results confirm the conclusion that the cluster structures we observed after cluster growth are ‘locked’, and that the observed Dh structure is metastable with respect to fcc.

In summary, Au₅₆₁ and Au₇₄₂ nanoclusters were produced under similar, slow growth formation conditions, and the proportions of structural isomers were determined by comparison of HAADF STEM images with electron scattering simulations. For both sizes the proportions of the main isomers are such that the decahedron is most abundant (Dh>fcc>Ih), but more importantly the relative abundances are the same in both cases and the same as for Au₉₂₃. On the basis of these experimental results, combined with the growth mechanisms found in molecular dynamics simulations and atomic manipulation experiments under the electron beam, which tend to convert Dh structures to fcc structures, we conclude that the atomic structures and their proportions observed at all these sizes are determined by template growth onto smaller, seed structures, the thermal energy available at the growth temperatures being insufficient to produce (local) equilibrium configurations. The combination of tools employed here can doubtless be applied to many other nanosystems, whether clusters, nanoparticles or beyond, to reveal the hierarchy of metastability that underpins the formation and applications of nanostructures.

References

1. Lu, J. et al. Coking- and sintering-resistant palladium catalysts achieved through atomic layer deposition. *Science* **335**, (2012).
2. Lu, K., Lu, L. and Suresh, S. Strengthening Materials by Engineering Coherent Internal Boundaries at the Nanoscale. *Science* **324**, (2009).
3. Bartels, T., Choi, J. G. and Selkoe, D. J. α -Synuclein occurs physiologically as a helically folded tetramer that resists aggregation. *Nature* **477**, 107-111, (2011).
4. Turner, M. et al. Selective oxidation with dioxygen by gold nanoparticle catalysts derived from 55-atom clusters. *Nature* **454**, 981-983, (2008).
5. Saha, K., Agasti, S. S., Kim, C., Li, X. and Rotello, V. M. Gold nanoparticles in chemical and biological sensing. *Chem. Rev.* **112**, 2739-2779, (2012).
6. Kim, C., Ghosh, P. and Rotello, V. M. Multimodal drug delivery using gold nanoparticles. *Nanoscale*, **1**, 61-67, (2009).
7. Chithrani, B. D. and Chan, W. C. W. Elucidating the mechanism of cellular uptake and removal of protein-coated gold nanoparticles of different sizes and shapes. *Nano Lett.* **7**, (2007).
8. Verdaguer-Casadevall, A. et al. Trends in the electrochemical synthesis of H₂O₂: enhancing activity and selectivity by electrocatalytic site engineering. *Nano Lett.* **14**, 1603-1608, (2014).
9. Campbell, C. T. The active site in nano particle gold catalysis. C. T. *Science* **306**, 234-235, (2004).
10. Desireddy, A. et al. Ultrastable silver nanoparticles. *Nature* **501**, 399-402, (2013).
11. Barnard, A. S., Young, N. P., Kirkland, A. I., Huis, M. A. and Xu, H. Nanogold: a quantitative phase map. *ACS Nano* **3**, 1431-1436, (2009).
12. Baletto, F., Ferrando, R., Fortunelli, A., Montalenti, F. And Mottet, C. Crossover among structural motifs in transition and noble-metal clusters. *J. Chem. Phys.* **116**, 3856-3863, (2002).
13. Kuo, C-L. and Clancy, P. Melting and freezing characteristics and structural properties of supported and unsupported gold nanoclusters. *J. Phys. Chem. B.* **109**, 13743-13754, (2005).
14. Li, Z. Y. et al. Three-dimensional atomic-scale structure of size-selected gold nanoclusters. *Nature* **451**, 46-49, (2008).
15. Wang, Z. W. and Palmer, R. E. Determination of the ground-state atomic structures of size-selected Au nanoclusters by electron-beam-induced transformation. *Phys. Rev. Lett.* **108**, (2012).

16. Koga, K. and Sugawara, K. Population statistics of gold nanoparticle morphologies: direct determination by HREM observations. *Surface Science* **529**, 23-35, (2003).
17. Clark, J. N. et al. Ultrafast three-dimensional imaging of lattice dynamics in individual gold nanocrystals. *Science* **341**, 56-59, (2013).
18. Plant, S., Cao, L. and Palmer, R. E. Atomic structure control of size-selected gold nanoclusters during formation. *J. Am. Chem. Soc.* **136**, 7559-7562, (2014).
19. Baletto, F. and Ferrando, R. Structural properties of nanoclusters: energetic, thermodynamic, and kinetic effects. *Reviews of Modern Physics* **77**, 371-423, (2005).
20. Krivanek, O. et al. Atom-by-atom structural and chemical analysis by annular dark-field electron microscopy. *Nature* **464**, 571-574, (2010).
21. Koch, C. PhD. Thesis, Arizona State University, (2002).
22. Gupta, R. P. Lattice relaxation at a metal surface. *Phys. Rev. B.* **23**, 6265, (1981).
23. Cyrot-Lackmann, F. and Ducastelle, F. Binding energies of transition-metal atoms adsorbed on a transition metal. *Phys. Rev. B.* **4**, 2406, (1971).
24. Baletto, F., Mottet, C. and Ferrando, R. Microscopic mechanisms of the growth of metastable silver icosahedra. *Phys. Rev. B.* **63**, 155409, (2001).

Acknowledgements We thank Kuo-Juei (Ray) Hu for his help with the electron scattering simulations, and checking of the image assignments. DMW is grateful for financial support from the EU project NanoMILE. We thank EPSRC for financial support of the experiments and acknowledge COST Action MP0903 NANOALLOY for networking support. The STEM instrument employed in this research was obtained through the Birmingham Science City project “Creating and Characterising Next Generation Advanced Materials,” supported by Advantage West Midlands (AWM) and in part funded by the European Regional Development Fund (EDRF).

Author Contributions DMW performed experiments and image assignments presented in the report. GR and RF conducted the growth simulations. REP designed the experiments. All authors contributed to the writing of the paper.

Author Information The authors declare no competing financial interests. Correspondence and requests for materials should be addressed to R.E.Palmer@bham.ac.uk.

Tables

Table 1. Results of the growth simulations

Growth temperature	Decahedral	Fcc	Icosahedral	Unclassified
400K	6	3	1	2
500K	7	4	0	1
600K	5	6	1	0
Total	18 (50%)	13 (36%)	2 (6%)	3 (8%)

Table 1. Results of the growth simulations. The proportion of Dh, fcc, Ih and unclassified clusters at T=400K, T=500K, T=600K, and the overall percentage of structures is shown.

Table 2. Frequency of structural transformations of Au₅₆₁ clusters irradiated with the STEM electron beam

Initial State	Intermediate State	Final State	Frequency
Dh	-	fcc	8
Dh	-	Dh	1
fcc	-	fcc	8
fcc	Dh	fcc	1

Table 2. The frequency of structural transformations of 18 Au₅₆₁ clusters continuously irradiated with the STEM electron beam while imaging. The initial state (the structure identified in the first images of the sequence) and final state (structure identified in the final images of the sequence) are shown together with (in one case) an intermediate state, alongside the frequencies of the different transition pathways.

Figures

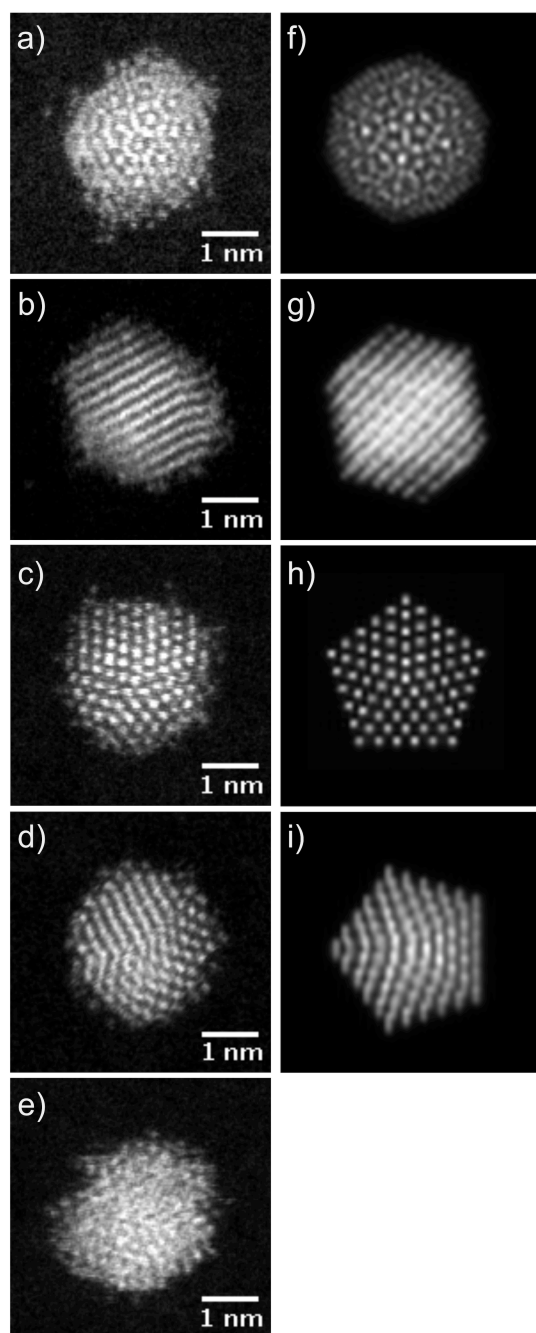


Figure 1. HAADF STEM images and corresponding electron scattering simulations for Au_{561} clusters.

(a)-(e) show HAADF STEM images of Au_{561} clusters with corresponding electron scattering simulations in (f)-(i): (a, f) Icosahedron (27,5) orientation, (b, g) cuboctahedron (fcc family) (15,60) orientation. (c, h) Ino-decahedron (Dh family) orientated along a five-fold axis (0,0). (d, i) Ino-Decahedron which not orientated on a high symmetry axis (18,10), and (e) an amorphous (unclassified) cluster.

The specific orientations (θ, α) of the model clusters used in the simulated images are given in Supplementary Fig. S1.

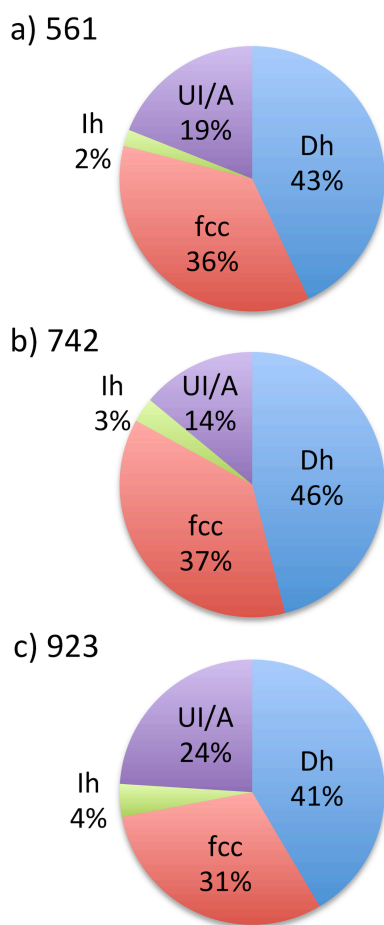


Figure 2. Percentages of structures observed for Au_{561} and Au_{742} compared with Au_{923}^{18} .

(a)-(c) show the percentage of structures observed for Au_{561} and Au_{742} compared with Au_{923}^{18} . Clusters are classified as face-centered-cubic (fcc), Decahedron (Dh), Icosahedron (Ih) or unidentified or amorphous (UI/A). The magnetron power, 10W, and condensation length, 250mm, were the same in all cases

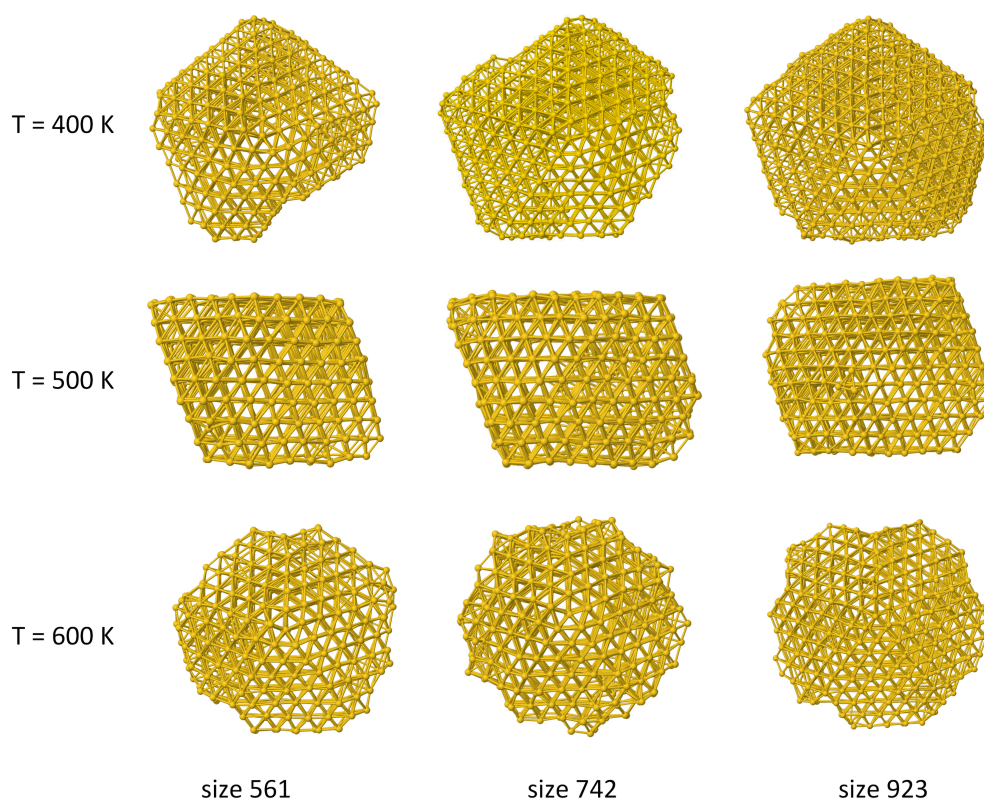


Figure 3. Snapshots from growth simulations at different temperatures.

T=400 K: growth of a decahedron. T=500 K: growth of an fcc truncated octahedron.

T=600 K: growth of a decahedron.

Methods

Production of nanoclusters

The gold nanoclusters employed in this work were produced by a magnetron sputtering, gas aggregation cluster beam source²⁵, and size selected using a lateral time of flight mass filter²⁶ (mass resolution of $M/\Delta M = 22$) to give clusters with 561 ± 13 atoms and 742 ± 17 atoms. The process is that gold atoms are sputtered from a polycrystalline by an argon plasma and clusters are formed by condensation in a helium (and argon) buffer gas cooled to $\sim 100\text{K}$. The positively charged clusters are focused into a beam and mass selected before deposition. The deposition energy of the clusters can be controlled by the accelerating voltage applied to the substrate. It is possible to influence the size and structure^{18, 25} of the clusters produced by changing the pressure in the condensation chamber, the condensation length and the sputtering power. In this work the nanoclusters were produced under slow growth conditions (low magnetron power, 10W, and long condensation length, 250mm) to reduce kinetic trapping of structures, and were soft-landed (for Au561 at either 2.7 or 1eV per atom, for Au742 at 2eV per atom)²⁷ onto a TEM grid coated with amorphous carbon to maintain their structure and avoid fragmentation. Clusters diffuse to defect sites on the surface where they are immobilized²⁷. The coverage was controlled by the beam current and deposition time chosen, to give a mono-dispersed sample, on which aggregation was negligible.

Characterisation using STEM

The samples were imaged using a 200 keV (JEOL 2100F) STEM with a spherical aberration corrector (CEOS) and resolution 0.1 nm. The HAADF detector inner collection angle was 62 mrad. This enabled the atomic structure to be determined¹⁴ via comparison with multiple electron scattering simulations²¹ for the icosahedron, Ino-decahedron and cuboctahedron; the simulation atlas method¹⁵.

Cluster growth simulations

Molecular-dynamics simulations of cluster growth were performed²⁴ by depositing atom by atom at a rate of 4.8 ns^{-1} . The nanoparticle temperature was kept constant during growth. Simulations started from a small seed of 13 atoms and reached a final size of 1000 atoms. Three growth temperatures (400, 500, and 600 K) were considered. The atomistic interaction potential used in the simulation is the Gupta potential²², which is based on the second-moment approximation to the tight-binding model²³. This potential reproduces correctly Au surface reconstructions²⁸. Its accuracy has been recently tested against the structures and local relaxations of Au nanoparticles on MgO(001)²⁹, obtaining very good agreement with the experiments. The structures of the growing clusters were classified using the common neighbor analysis method³⁰.

Method reference list

25. Pratontep, S., Carroll, S. J., Xirouchaki, C., Streun, M. and Palmer, R. E. Size-selected cluster beam source based on radio frequency magnetron plasma sputtering and gas condensation. *Review of Scientific Instruments* **76**, 045103-1-9, (2005).
26. Von. Issendorff, B. and Palmer, R. E. A new high transmission infinite range mass selector for cluster and nano particle beams. *Review of Scientific Instruments* **70**, 4497-4501, (1999).
27. Di Vece, M., Palomba, S. and Palmer, R. E. Pinning of size-selected gold and nickel nanoclusters on graphite. *Phys. Rev. B.* **72**, 073407-1-4, (2005).
28. Guillopé, M. and Legrand, B. (110) Surface stability in noble metals. *Surf. Sci.* **215**, 577-595, (1989).
29. Han, Y., Ferrando, R. and Li, Z. Y. Atomic details of interfacial interaction in gold nanoparticles supported on MgO(001). *J. Phys. Chem. Lett.* **5**, 131-137, (2014).
30. Faken, D. and Jonsson, H. Systematic analysis of local atomic structure combined with 3D computer graphics. *Comp. Mat. Sci.* **2**, 279-286, (1994).